JOURNAL OF AIRCRAFT
Vol. 46, No. 6, November–December 2009

Collision Detection System Based on Differential Carrier-Phase Global Positioning System Broadcasts

Soon Sik Hwang* and Jason L. Speyer†
University of California, Los Angeles, Los Angeles, California 90095-1597

DOI: 10.2514/1.43517

The Global Positioning System has great potential for the development of new collision avoidance systems and is being considered for the next-generation traffic alert and collision avoidance system. The navigation states estimated by Global Positioning System code information can be broadcast to nearby airplanes via the current traffic alert and collision avoidance system equipment. In this paper, the problem of aircraft collision detection system using Global Positioning System carrier-phase information is addressed. A new approach to the carrier-phase-based relative position estimation problem is proposed that uses particle filters in which the samples are drawn from Cartesian position space coordinates. The particle filters with position samples makes the Global Positioning System carrier-phase-based position estimation algorithm robust and practical in that the algorithm is not sensitive to changes of Global Positioning System satellites and cycle slips. The same algorithm can be used to estimate the vehicle attitude if multiple Global Positioning System antennas are used. For a reliable and enhanced collision avoidance system, three-dimensional trajectories are projected using relative position, velocity, and attitude estimates. It is shown that the performance of the Global Positioning System carrier-phase-based collision-detecting algorithm meets the accuracy requirements for a precise approach of flight with significantly less collision false alarms and no miss alarms.

Nomenclature

A	=	transition matrix between the body frames and inertial frames
c	=	velocity of light
Eu	=	attitude expressed as Euler parameters (roll, pitch, and yaw)
$\mathbf{E}_X[Y]$	=	expectation function of Y over the probability density function X
$H_{i'}$	=	direction matrix to all visible Global Positioning System satellites at the linearized point $X_{i'}$
$H_{i'}^{(j)(k)}$	=	direction matrix at the linearized point $X_{i'}$ to the GPS satellites l ($l = j, \ldots, k$)
$I_{(j)}^{(i)}$	=	ionospheric delay error
$Mp_{(j)}^{(i)}, mp_{(j)}^{(i)}$	=	code and carrier-phase multipath error
m_s	=	number of samples
$N_{(j)}^{(i)}$	=	integer cycle ambiguity
$\tilde{N}_{(j)}^{(i)}$	=	estimated real ambiguity
n_a	=	number of antennas
n_s	=	number of available Global Positioning System satellites
$n_{(j)}^{(i)}, \eta_{(j)}^{(i)}$	=	code and carrier-phase noise error
$p(X\|Y)$	=	conditional probability density function of X given Y
$p_{(j)}^{(i)}, \phi_{(j)}^{(i)}$	=	measured code and carrier phase in range
$\mathbf{q}$	=	quaternion expressed as the vector $[q1 \quad q2 \quad q3 \quad q4]$
$r(t_c)$	=	measured relative distance between aircraft 1 and 2 at current time
$r_{\text{pred}}(t_c)$	=	predicted relative distance between aircraft 1 and 2 at current time
$S^{(i)}$	=	ephemeris error of Global Positioning System satellite i
$T^{(i)}$	=	clock error of Global Positioning System satellite i
$Tr_{(j)}^{(i)}$	=	tropospheric delay error
$t_{(j)}$	=	clock error of receiver j
UPR^i	=	approximation of uncertainty prediction region, $i = 1, \ldots, m_s$
V_i	=	inertial velocity of aircraft i ($i = 1, 2$)
$\bar{X}, \Omega_X$	=	mean and variance of X
$\tilde{X}$	=	estimation of X
X_i	=	inertial position of aircraft i expressed as the vector $[x_i \quad y_i \quad z_i]^T$ ($i = 1, 2$)
x_k^i	=	sample i for state x_k at discrete time k
$z_{1:k}$	=	measurement history up to time k
$\boldsymbol{\alpha}$	=	angular acceleration
δX_i	=	baseline vector between secondary antenna i and primary antenna on the same airplane
λ	=	carrier wavelength
$\rho_{(j)}^{(i)}$	=	geometric range
$\boldsymbol{\omega}_{(j)}$	=	angular velocity of aircraft j expressed as the vector $\{\omega_x, \omega_y, \omega_z\}^T$
$(\cdot)_{(j)}^{(i)}$	=	parameter about aircraft j associated with Global Positioning System satellite i

I. Introduction

THE current midair collision avoidance system uses range-based sensors such as primary surveillance radar, secondary surveillance radar, and a traffic alert and collision avoidance system (TCAS). TCAS provides distance measurements, altitude information, etc., between airplanes. However, the current TCAS cannot provide full three-dimensional information [1]. Great benefits are achievable from the Global Positioning System (GPS) such as accuracy and coverage with minimum system size. One negative aspect of the current TCAS is the number of unnecessary alarms [i.e., false alarms (FAs) and unnecessary resolution advisories (RAs) [2]]. Because FA induces RA, and the RA can induce a conflict, the FA can become as risky as miss alarms (MAs).

Collision detection algorithms using GPS have been studied, but they are based only on GPS code information [3,4]. The GPS code estimates of position can be used for level-flight airplanes, but carrier-phase (CP)-based navigation systems are essential to meet the

Received 29 January 2009; revision received 12 April 2009; accepted for publication 12 April 2009.

*Research Assistant, Department of Mechanical and Aerospace Engineering. xpluxmea@ucla.edu.

†Professor, Department of Mechanical and Aerospace Engineering. speyer@seas.ucla.edu. Fellow AIAA.

category III accuracy requirements in a precision approach for autolanding guidance in the terminal area [1]. To make use of CP in the relative position estimation problem, the integer number of wavelengths between antennas, called the integer ambiguity problem, should be resolved. The traditional approach to the integer-ambiguity-resolution problem is to search for the correct integer from a set of integers hypotheses. The integer ambiguity should be resolved before there is any changes in the GPS satellites that are visible. Moreover, even after the integer ambiguity is resolved, the estimation accuracy is degraded when a cycle slip occurs in the phase-lock loop tracking due to 1) signal blocking by objects, 2) high acceleration of aircraft, 3) reflected signal (i.e., multipath), and 4) weak signal-to-noise ratio [5]. The carrier-smoothed-code method and triple-difference CP technique were introduced as CP navigation algorithms that meet the category III accuracy requirements [6]. The CP-smoothed-code method achieves better measurements by averaging the code [7] and CP measurements, and the triple-difference technique eliminates the integer ambiguity by differencing CP measurements between two epochs [8]. Both methods estimate the position with no ambiguity-resolution process. However, the convergence time for achieving the category III position precision is much longer and the accuracy decrease is more severe than the ambiguity-resolving algorithms when a cycle slip occurs. Note that for relative position estimation, both vehicles should use the same GPS satellites.

Hypotheses-testing algorithms have been widely used to solve this integer-ambiguity-resolution problem [9]. These algorithms are based on procedures that distinguish the correct integer ambiguity hypothesis from all other integer hypotheses. In contrast, we suggest the particle filter (PF) approach [10], in which the probability density function (pdf) of states is approximated for resolving the integer ambiguity and estimating the relative position. The PF is applied to a GPS CP-based navigation system in which the PF is supplied by samples drawn from position space. Because the position sample (PS) CP GPS (PS-CP-GPS) navigation algorithm estimates the pdf of the position states, the changes of integer ambiguity by changes of available GPS satellites constellation or cycle slips do not effect the PS-CP-GPS algorithm. The proposed algorithm is more robust and stable compared with the traditional ambiguity hypothesis techniques, and coherent estimation is achieved efficiently in real time in the presence of cycle slips and changes in the number of satellites.

The collision detection problem becomes quite complicated when the aircraft (A/C) start to change their heading directions. In that case, the attitude information is useful for estimating the future trajectory of the A/C, for which the velocity vector varies with the attitude of A/C. The PF-based relative position estimation technique is extended to the attitude determination problem for airplanes that are equipped with multiple GPS antennas. The benefits of the position samples also hold for the attitude determination problem. The number of states of relative position to be estimated becomes minimum with the position samples (5 position states for $n_a > 2$ antennas). The estimated relative position vectors, or baseline vectors, are transformed into attitude parameters (i.e., quaternion and Euler angles).

Finally, a collision-detecting scheme is established using the estimated relative position, velocity, and attitude parameters. The position and velocity of the intruders are estimated based on the transmitted CP measurements. The attitude parameters estimated in each aircraft's navigation system are transmitted as well as the CP measurements. The data link connection is shown in Fig. 1.

The projected region is constructed based on the mean and variance of the states estimated from the PF. The probability of a collision is determined from Monte Carlo (MC) analysis. Then we demonstrate the benefits of the PS-CP-GPS collision detection system as the new GPS-based TCAS (TCAS IV) and compare it with two kinds of collision detection systems [i.e., current TCAS system (TCAS II) and the system using automatic dependent surveillance–broadcast (ADS-B) information (ADSB system)] in terms of the FA and MA rates through simulations. The details of each system, such as the required information and algorithms used for collision detection, are described in Sec. III.

This paper is organized as follows. In Sec. II, we discuss the relative position and velocity estimation problem using the GPS code and CP measurements. The form of the particle filter is presented, which makes the CP GPS algorithm robust when the particle samples are obtained from a position space. The collision detection algorithm using the PS-CP-GPS particle filter is described in Sec. III, and simulation results are provided. Finally, we conclude in Sec. IV.

II. Relative Position Estimation Between Two Antennas

A. GPS Measurements

In this section, the algorithm of using a PF for PS-CP-GPS problem is discussed, the derivation of the PS-CP-GPS algorithm is mainly focused on in this paper, and details on accuracy and robustness are discussed more in the literature [11].

GPS receivers provide a pseudorange that is related to the measured travel time, called the code measurement, and is tracked in the code loop of the GPS receiver. The code measurement $p_{(j)}^{(i)}$ contains the range between the GPS antenna j and the ith GPS satellite along with several uncertainties:

$$p_{(j)}^{(i)} = \rho_{(j)}^{(i)} + S^{(i)} + c(t_{(j)} - T^{(i)}) + I_{(j)}^{(i)} + Tr_{(j)}^{(i)} + Mp_{(j)}^{(i)} + n_{(j)}^{(i)} \tag{1}$$

The CP is tracked in the phase-lock loop of the GPS receiver and gives information on range to the GPS satellite as well as velocity (Doppler shift). Similar to the code, the CP measurements $\phi_{(j)}^{(i)}$ can be modeled as

$$\phi_{(j)}^{(i)} = \rho_{(j)}^{(i)} - \lambda N_{(j)}^{(i)} + S^{(i)} + c(t_{(j)} - T^{(i)}) - I_{(j)}^{(i)} + Tr_{(j)}^{(i)} + mp_{(j)}^{(i)} + \eta_{(j)}^{(i)} \tag{2}$$

To construct measurements between two antennas, each absolute measurement in Eqs. (1) and (2) is differenced. The common errors in the measurements are assumed to be canceled out by differencing between the measurement equations, but uncommon errors, such as noise and multipath error, cannot be canceled out.

If the baseline between antennas is long (100–300 km), the ionospheric and tropospheric delay errors cannot be considered as common errors between antennas. Corrections to these errors can be made if we assume that the ionospheric and tropospheric delay errors are modeled as a Klobuchar model and Hopfield model, respectively, and can therefore be eliminated or ignored [8].

Multipath error has a major effect on degrading the accuracy in CP GPS positioning estimation and on the success of finding the correct integer ambiguity for the integer-ambiguity-resolution algorithms. The multipath error is usually modeled as a sinusoidal oscillation. If the geometry between GPS satellites and reflector does not change quickly, the multipath error appears as a bias over short time periods. To simulate the effect of the multipath error on the PF estimates, we introduce a bias to represent the multipath error to the CP measurements.

B. Difference Operation

For the short-baseline case (i.e., the baseline length is less than 100 km), many errors such as $S^{(i)}$, $c(t_{(1)} - T^{(i)})$, $I_{(1)}^{(i)}$, and $Tr_{(1)}^{(i)}$ in the observation in Eqs. (1) and (2) are considered to be a common error associated with both antennas and assumed to be eliminated or reduced by double-difference (DD) operation. In DD, the measurements for two antennas from one satellite are subtracted, and then that measurement for two satellites is again subtracted. The DD measurements for the code and CP between antennas 1 and 2 and GPS satellites i and j are defined as

$$\nabla\Delta p_{(12)}^{(ij)} \triangleq (p_{(2)}^{(i)} - p_{(1)}^{(j)} - (p_{(2)}^{(i)} - p_{(1)}^{(i)}) \approx \nabla\Delta p_{(12)}^{(ij)} + \nabla\Delta M p_{(12)}^{(ij)} + \nabla\Delta n_{(12)}^{(ij)} \tag{3}$$

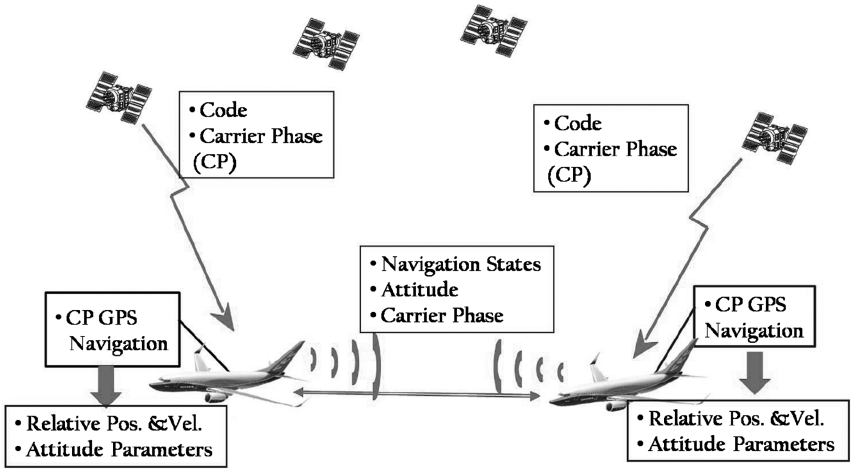

Fig. 1 Communication for data link.

$$\nabla\Delta\phi_{(12)}^{(ij)} \approx \nabla\Delta\rho_{(12)}^{(ij)} - \nabla\Delta\lambda N_{(12)}^{(ij)} + \nabla\Delta mp_{(12)}^{(ij)} + \nabla\Delta\eta_{(12)}^{(ij)} \quad (4)$$

$$\mathbf{E}\,[\nabla\Delta n_{(12)}^{(ij)}] = \mathbf{E}[\nabla\Delta\eta_{(12)}^{(ij)}] = 0 \quad (5)$$

where $\mathbf{E}[\cdot]$ represents the expectation.

The measurements equation in the vector form for all visible GPS satellites i and j in common can be rearranged as

$$\nabla\Delta P = [\,\nabla\Delta p_{(12)}^{(12)} \quad \nabla\Delta p_{(12)}^{(23)} \quad \cdots \quad \nabla\Delta p_{(12)}^{(n_s-1n_s)}\,]^T$$
$$\nabla\Delta\Phi = [\,\nabla\Delta\phi_{(12)}^{(12)} \quad \nabla\Delta\phi_{(12)}^{(23)} \quad \cdots \quad \nabla\Delta\phi_{(12)}^{(n_s-1n_s)}\,]^T \quad (6)$$

$$\mathrm{cov}\,[\nabla\Delta P] = \Omega_P, \qquad \mathrm{cov}[\nabla\Delta\Phi] = \Omega_\Phi \quad (7)$$

where cov[·] represents the covariance operator.

Equation (4) has the DD ambiguity term $\nabla\Delta N_{(12)}^{(ij)}$. After the DD ambiguity is known, Eq. (4) can be used for much more precise measurements than with the code. However, this unknown integer ambiguity cannot be computed directly in this form, because the term $\nabla\Delta\rho_{(12)}^{(ij)}$ is not known either. Therefore, the hypothesis tests over the ambiguity candidates are usually employed [12].

From this point on, we only use $\nabla\Delta$ or ∇ symbols as DD or single-difference values, respectively, and omit the $(\cdot)_{(12)}^{(ij)}$ symbol.

C. Initialization

To obtain an initial position, code information is used. The estimate of the absolute position of antenna 1 (X_1) can be obtained by a least-squares method using undifferenced code measurements from Eq. (1):

$$P_{(1)} - \varrho_{(1')} = \mathbf{A}\delta\hat{X}_1 + \mathbf{n} \quad (8)$$

where

$$\varrho_{(1')} = [\,\rho_{(1')}^{(1)} \quad \rho_{(1')}^{(2)} \quad \cdots \quad \rho_{(1')}^{(n_s)}\,]^T, \qquad \mathbf{A} = [\,H_{1'}^T \quad 1\,]$$
$$P_{(1)} = [\,\rho_{(1')}^{(1)} \quad \rho_{(1')}^{(2)} \quad \cdots \quad \rho_{(1')}^{(n_s)}\,]^T, \qquad \delta\hat{X}_1 \triangleq [\,\delta X_1 \quad c\cdot t_{(1)}\,]^T$$

where δX_1 is the difference between a linearization point $X_{1'}$ and X_1, $\varrho_{(1')}$ is a undifferenced range vector from $X_{1'}$ to all GPS satellites, and $\mathbf{n}$ is the vector of error terms including the common errors, multipath, and noise. The estimation of X_1 is given as $\tilde{X}_1 = X_{1'} + \delta\tilde{X}_1$, where $\delta\tilde{X}_1$ can be obtained by the least-squares method as

$$[\,\delta\tilde{X}_1 \quad \tilde{t}_{(1)}\,]^T = (\mathbf{A}^T\mathbf{A})^{-1}\mathbf{A}^T(P_{(1)} - \varrho_{(1')}) \quad (9)$$

For a short baseline, the estimation $\tilde{X}_1$ will be taken as the true position value for X_1, and then the relative positioning problem comes down to estimating the relative position between $\tilde{X}_2$ and X_1. The initial estimation of $\tilde{X}_2$ is required as an initial condition for the PF. The DD code information can be used for the initial value of $\tilde{X}_2$:

$$\nabla\Delta P - \nabla\Delta\varrho_{2'} = \mathbf{A}_d\delta X_2 + \nabla\Delta\mathbf{n} \quad (10)$$

$$\mathbf{A}_d = [H_{2'}^{(2)(n_s)} - H_{2'}^{(1)(n_s-1)}]^T \quad (11)$$

where $X_{2'}$ is an arbitrary linearization point for X_2, δX_2 is a relative position between X_2 and $X_{2'}$, and

$$\nabla\Delta\varrho_{2'} = [\,\nabla\Delta\rho_{(12')}^{(12)} \quad \nabla\Delta\rho_{(12')}^{(23)} \quad \cdots \quad \nabla\Delta\rho_{(12')}^{(n_s,n_s-1)}\,]^T$$

Then the estimation of the position of antenna 2 by the DD code is given by $\tilde{X}_2 = X_{2'} + \delta\tilde{X}_2$, where

$$\delta\tilde{X}_2 = (\mathbf{A}_d^T\Omega_\Phi^{-1}\mathbf{A}_d)^{-1}\mathbf{A}_d^T\Omega_P^{-1}(\nabla\Delta P - \nabla\Delta\varrho_{2'}) \quad (12)$$

The initial velocity can be computed directly from the Doppler shift measurements:

$$\nabla\varphi_{(k)}^{(ij)} = [H_k^{(j)}\cdot V^{(j)} - H_k^{(i)}\cdot V^{(i)}] + [H_k^{(i)(j)}\cdot V_k], \qquad k = 1, 2 \quad (13)$$

where $H_k^{(i)}$ is the direction matrix between antenna k and GPS satellite i, V is the velocity vector, and $\nabla\varphi$ is the vector form for the single-difference Doppler shift measurements of antenna k.

D. Position Sample Particle Filter

We present our approach to handling the CP integer-ambiguity-resolving problem with the PF. More details of the constructing PF for CP measurements are given in [11]. We denote the sampled particles from the initial pdf of states at time $k = 0$ as $x_0^i \sim p(x_0|z_0)$ $(i = 1, \ldots, m_s)$. Each sample x_k^i is a 6 by 1 vector and represents a realization of position and velocity for antenna 2, $[\,X_2 \quad V_2\,]$, in the ECEF coordinates. Therefore, the samples x_k^i $(i = 1, \ldots, m_s)$ can be obtained by picking m_s number of independent points in three-dimensional position space and velocity space. The distribution of samples can be assumed to be Gaussian or uniform. The mean is estimated in Sec. II.C, and the variance is given by a priori statistics.

Building the likelihood pdf for the states $p(z_k|x_k^i)$ is the most important part of the PS-CP-GPS algorithm. To develop the PF algorithm using the position space samples, consider the DD CP measurements:

$$\nabla\Delta\varrho = \nabla\Delta\Phi + \lambda\cdot\nabla\Delta N + \nabla\Delta\eta \quad (14)$$

where $\nabla\Delta\varrho$ is the vector of the DD geometric range between satellites and X_1, X_2. Equation (14) can be linearized around $\tilde{X}_2$ by using estimates in Eq. (12):

$$\nabla\Delta\varrho_o + A_d\delta X_2 = \nabla\Delta\Phi + \lambda\cdot\nabla\Delta N + \nabla\Delta\eta \tag{15}$$

We use both the nonlinear version of the measurement equation (14) and the linearized version of the measurement equation (15). The given particles will be applied to the nonlinear equation (14).

Before we use the nonlinear measurements equation, an estimate of the integer ambiguity, $\nabla\Delta N$, is to be made. Consider an annihilator E constructed from the left null space of the direction matrix A_d:

$$E = \text{null}(A_d^T) \tag{16}$$

such that $E^T\cdot A_d = 0$. The notation null$(\cdot)$ defines the null space of $(\cdot)$. This annihilator of A_d is not unique, but exists when the row number of A_d is greater than four. Multiplying E^T on both sides of Eq. (15) and rearranging provide

$$E^T\cdot\nabla\Delta N_L \triangleq E^T(\nabla\Delta\varrho_0 - \nabla\Delta\Phi - \nabla\Delta\eta)/\lambda \tag{17}$$

Define $\nabla\Delta N_L$ as an ambiguity from the linearized measurements from Eq. (17). Because the position-dependent term is eliminated, Eq. (17) is independent of the position samples. However, the ambiguity $\nabla\Delta N_L$ is not integer-valued because of $\nabla\Delta\eta$. If we could find any integer ambiguity that is close to $E^T\cdot\nabla\Delta N_L$ when projected by the left annihilator E^T, then the probability of being the true integer ambiguity is high. From Eq. (14), the integer ambiguity is computable if $\nabla\Delta\varrho$ is given. In fact, a position part of each sample x^i can be substituted for X_2, and therefore m_s samples basically generate m_s DD ranges between X_1 and the position part of each particle's x_k^i $(\nabla\Delta\varrho^i)$. The float ambiguity estimates for each position sample's x_k^i are computed using $\nabla\Delta\varrho^i$ from Eq. (14) as

$$\nabla\Delta\tilde{N}^i \triangleq \frac{1}{\lambda}\nabla\Delta(\varrho^i - \Phi) \tag{18}$$

When the integer property of the ambiguity is applied, the expected estimates of the integer ambiguities corresponding to each sample can be obtained by rounding off as

$$\nabla\Delta\underline{N}^i \triangleq [\nabla\Delta\tilde{N}^i]_{\text{round off}} \tag{19}$$

These integer-valued ambiguities are compared with the ambiguity estimate $\nabla\Delta N_L$ from the linearized equation (17). By the round-off operation, the integer ambiguity estimate $\nabla\Delta\underline{N}^i$ for the ith sample is independent of the noise under the assumption that the summation of the DD noise $\nabla\Delta\eta$ and a portion of common error assumed to be eliminated in the DD measurements is less than $\lambda/2$ ($\approx$19/2 cm: L_1 frequency CP). Because the common errors are assumed to be ignorable in the short-baseline case, this assumption holds as long as the summation of the uncommon error (noise and multipath) does not exceed $\lambda/2$. However, it is not trivial to check the magnitude of the noise and multipath in the DD measurements. We take care of the effect of the noise and multipath by simulation. Each sample position provides an integer ambiguity, but only one of the integer ambiguities is the true integer ambiguity, because the samples far from true position will provide the wrong integer value.

If the noise in the measurements is assumed to be Gaussian, the conditional pdf $p(z_k|x_k^i)$ can be modeled as

$$p(z_k|x_k^i) = C_1\exp\{-\tfrac{1}{2}(r^i)^T(E^T\Omega_\Phi E)^{-1}(r^i)\} \tag{20}$$

where the residual is

$$r^i = \lambda E^T(\nabla\Delta\underline{N}^i - \nabla\Delta N_L) \tag{21}$$

In the frame of sequential importance sampling [10] PF, the update of weight can be expressed with the given pdf of each sample in Eq. (20) as

$$\underline{w}_k^i = \frac{\underline{w}_{k-1}^i C_1\exp\{-\frac{1}{2}(r^i)^T(E^T\Omega_\Phi E)^{-1}(r^i)\}}{\sum_{j=1}^m \underline{w}_{k-1}^i C_1\exp\{-\frac{1}{2}(r^j)^T(E^T\Omega_\Phi E)^{-1}(r^j)\}} \tag{22}$$

The expectation of the position at time k with the sequentially updated weights in Eq. (22) can be obtained as

$$\mathbf{E}[(x_k)] = \sum_{i=1}^{m_s}(x_k^i)\underline{w}_k^i \tag{23}$$

Finally, samples x_{k+1}^i drawn according to the importance density

$$q(x_{k+1}|x_k^i, z_{1:k}) = p(x_{k+1}|x_k^i)$$

can be used for evaluating the weight of particles at time $k+1$ using Eq. (22) for the resampling step of the PF.

E. Precise PF Position Estimates Results

A simulation was implemented for evaluating the estimates of the relative position of airplanes in flight in the vicinity of Los Angeles International Airport. The basis for our experiments was a sequence of GPS satellite positions and a sequence of simulated positions of two airplanes communicating with each other. The orbit tracks of the GPS satellites were obtained from the International GNSS Service for 19 November 2007.[‡] The measurements received by GPS receiver were generated at a 2 Hz rate. The two airplanes in level flight have a baseline of 5 km (16,404 ft) and are approaching each other (i.e., the velocities of both airplanes are constant and no forces are applied). Eight GPS satellites were available during simulation time.

The generated data included the ionospheric and tropospheric delay errors, ephemeris errors, and clock errors. Ionospheric distortion based on the Klobuchar model was imposed on the code and CP measurements, with the experienced total electron count varied between a minimum of 4×10^{16} and a maximum of 1.6×10^{17} [13]. The humidity used in the Hopfield model for tropospheric delay error was 80%.

With regard to the noise, the range measurement accuracy is assumed to be 3 m and 3 cm in magnitude for the code and CP, respectively. The multipath error is treated as an additional bias term for which the size is less than 2 cm and corrupts the CP measurements in the simulation.

The PF introduced in a previous paper [11] is applied to the estimation of the relative position of the airplanes using GPS CP information. The sampling process is implemented for obtaining the initial samples. A uniform distribution is used for the initial samples and the weights $\{x^i, \underline{w}^i, i = 1,\ldots,m\}$. The reason for choosing the uniform distribution is that if the initialization process of the PF is over only one time period, then the initial state estimated by the code measurements is usually not precise enough to be used directly for the initial conditions of the CP measurements-based filter. Therefore, using the normal distribution of the initial weight may take more time to converge.

The performance analysis of the proposed PF with position-based samples is compared with the ambiguity-based algorithm with respect to three-dimensional relative position error. The relative position accuracy is compared with the ambiguity-based case in the following way. For the position estimates of the ambiguity-based algorithm, the true integer ambiguity is assumed to be fixed and given to the CP measurements equation (2). Then two nonlinear filtering techniques, the unscented Kalman filter (UKF) and the extended Kalman filter (EKF), are applied for the nonlinear observation equations of Eq. (14). Therefore, these filters operate on CP measurements assuming that the ambiguity-based algorithm has succeeded in resolving the true integer ambiguity.

There is no change of the GPS satellites or the cycle slip occurring during this chosen experiments so that only positioning accuracy can be compared, rather than the comparison of the time required for searching the correct integer ambiguity or the success rate of the searched integer ambiguity. However, the position estimates were not affected by the cycle slip, and the details of the effect of cycle slips or

[‡]Data available online at http://igscb.jpl.nasa.gov/ [retrieved 3 May 2009].

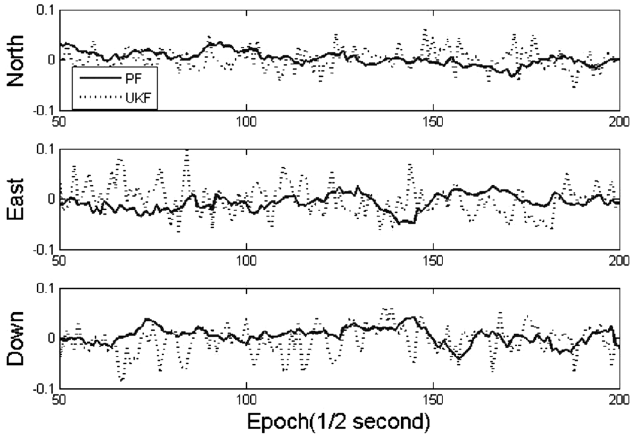

Fig. 2 Three-dimensional position error: ambiguity-fixed (UKF) and position-based (PF).

changes on the PS-CP-GPS PF results are discussed in a previous paper [11].

For analysis purposes, the positioning results for The PF and UKF are shown in Fig. 2. The solid line and dotted line represent the error in the position estimates for the PF and UKF, respectively.

The position accuracy between the UKF estimates with fixed ambiguity and the PF with position-based samples are compared in Table 1. The results show that the proposed PF is comparable with the estimates of the UKF with fixed ambiguity. The UKF and EKF produced identical results.

F. Attitude Determination

Attitude determination is based on the multiple-baseline vectors, which are the relative position vectors between the GPS antennas i $(i = 0, \ldots, n_a)$ on each aircraft. A multiple number of baselines increases the difficulty of the attitude determination problem with respect to the elapsed time to search for the correct integer ambiguities, and the number of integer ambiguity hypotheses increases as the number of baseline increases. For that reason, most of the CP-based attitude determination algorithms limit the number of baseline vectors to four. The PS-CP-GPS particle filter discussed in Sec. II is employed for estimating the baseline vectors of the multiple antennas on one A/C. The beauty of sampling from the position space instead of from the integer ambiguity space is that $n_B > 2$ baseline vectors can be directly expressed in terms of relative positions with a known antenna's geometry (see Appendix A).

The attitude determination algorithm using the PF with position samples can be implemented in two stages. First, n_B baseline vectors are estimated in the PF. Second, the transition matrix from a body frame to a inertial frame is determined as a function of quaternion or Euler angles. This procedure is discussed in Appendix A. This attitude parameters are to be transmitted among A/C to improve the performance of the TCAS IV.

III. Collision Detection/Avoidance System

Noncooperative sensors such as radar (radio detection and ranging) have been widely used as major sensors for collision avoidance systems. Such systems have the capability of measuring distance and the rate of change of the distance to a nearby aircraft. All current commercial and military aircraft are at least equipped with TCAS I, which is based on the use of transponders. These transponders interrogate within a range of 30 n mile at a 1 Hz frequency. The other TCAS-equipped transponders emit the response signal to the interrogator and simultaneously to the ground-based air traffic control system with altitude information. The time differences between interrogating and the arrival time of the respond signal generate the range measurements. The range measurements and the altitude information can be used to determine the relative distances and relative vertical speeds between the interrogator aircraft and other nearby mode A or C transponder-equipped aircraft. The current TCAS II system is equipped with a mode-S transponder that is capable of broadcasting [i.e., extended mode-S (1090 ES)]. Each airplane can periodically broadcast the navigation information using the extended mode-S transponder, called *squitter*. This concept is called automatic dependent surveillance–broadcast. The communication by ADS-B is considered to be an important technology for distributed air/ground traffic management by NASA. After the Federal Aviation Administration (FAA) abandoned developments of the TCAS III due to inaccuracy of the bearing measurements, TCAS IV has replaced TCAS III as a next-generation TCAS. The next-generation collision detection systems have three-dimensional monitoring capability by combining the GPS navigation information in the broadcasting message. For the desired performance of future air traffic control such as the free-flight project, the navigation information such as the GPS CP measurement, 3-D position, velocity, and attitude parameters should be available among airplanes. CP-based differential GPS navigation system can meet the category III accuracy (horizontal accuracy: 4.1 m or 13.44 ft, vertical accuracy: 0.5 m or 1.64 ft) requirements for precision approaches, which is re not generally the case by using only GPS code information [13]. We propose the GPS-CP-based collision detection system as a next-generation TCAS system. The own airplane keeps tracking its navigation states and broadcasts those states to the nearby airplanes.

The revised standard performance of ADS-B, addressed in RTCA/DO-242A [14], introduces the expansion of message parameters, so-called intent parameters [15]. The future trajectories of the airplane can be predicted according to the information in ADS-B reports such as the target states (i.e., target position and heading) and the trajectory change point (i.e., trajectory type, heading, and turn rates). These ADS-B reports, so-called intent reports, for surveillance are useful for generating trajectories of nearby airplanes.

In this section, three ground-independent collision detection systems are considered in which the systems are characterized by the available data types. The performance of each system is analyzed for two modes of flight: constant-velocity flight mode and maneuvering flight mode, in which the velocity vector of the A/C changes direction. The first collision detection system is range-based and altitude-combined collision detection (TCAS II). TCAS II makes use of the relative range measurement and the received altitude of own and intruder. The second system is a GPS-based collision detection system (TCAS IV). The available data for this detection system are three-dimensional position, velocity, attitude parameters, and the GPS CP measurements transmitted and received by various surveillance communication links. The third is an ADSB-based collision detection system. The ADSB-based system is assumed to follow the document RTCA/DO-242A [14] for its transmission data protocol. The essential data for the ADSB detection system are the horizontal states (horizontal position and speed, heading angle, and turn rates) and vertical state (altitude). Therefore, the TCAS II is a two-dimensional system (range and altitude), the ADSB-based system is three-dimensional (the horizontal information is decoupled from the vertical information), and the TCAS IV is also three-dimensional (the states are fully coupled

Table 1 Position estimates: accuracy comparison

	Mean Error	NED[a]	RMS Error	NED[a]
Fixed ambiguity, cm	0.09 −0.72	0.54	2.18 3.20	2.87
Position-based samples, cm	−0.73 −0.18	0.59	1.36 1.18	0.97

[a]N is north, E is east, and D is down.

in the horizontal and vertical directions). For the maneuvering flight, the FA rate is determined by a combination of many factors, and it cannot be analyzed in terms of the miss distance or relative velocity explicitly. Therefore, the maneuvering velocity case is discussed separately to represent the performance of FA rate in terms of the relative velocity and miss distance.

Because the collision detection system is designed to be cautious so that a mishap cannot occur without any alarm, the current detection system is prone to produce many FAs. Our main goal is to address the strength and efficiency of the GPS-based collision detection system over TCAS II and ADSB-based detection systems in terms of FA and MA rates.

A. Constant-Velocity Flight

Collision prediction is based on the position after prediction time t_{pred}, which is estimated using the current position and velocity [16]. To discuss the performance and alarm rate of the collision detection systems, TCAS II and TCAS IV are addressed, in which the A/C approaches with constant velocity are considered. The algorithm of ADSB-based collision detection system is identical to the TCAS IV when a velocity of A/C is a constant vector and turning motions for the horizontal and vertical directions are not coupled. Therefore, the ADSB-based collision detection system is not discussed for the constant-velocity flight, but will be considered for the maneuvering flight in Sec. III.B.

1. TCAS II

A potential collision between aircraft can be detected in either the time test or range test [17]. Because the bearing measurement of TCAS II to other aircraft is not accurate enough, it is not used in collision avoidance algorithms [13]. The point at which both A/C are the closest in the approach track, closest point of approach (CPA), between own A/C (A/C 1) and intruder (A/C 2) cannot be estimated accurately by TCAS II except for the constant-velocity flight. Instead, the test is often given by a time criterion, called the Tau criterion, to issue an advisory to a pilot in a timely way. The time test monitors time-to-go as [18]

$$\frac{r(t_c)}{-\dot{r}(t_c)} = t_{\text{pred}} < \text{Tau}, \qquad \frac{r_z(t_c)}{-\dot{r}(t_c)} = t_{\text{pred},z} < \text{Tau} \tag{24}$$

where $r_z(t_c)$ represents a vertical relative distance; $\dot{r}(t_c)$ and $\dot{r}_z(t_c)$ are the rates of range of r and r_z, respectively, at t_c; and t_{pred} and $t_{\text{pred},z}$ are used as the approximation of the time to the horizontal and vertical CPA, respectively. The test determines when to trigger an alarm when t_{pred} or $t_{\text{pred},z}$ is less than the Tau criterion provided by TCAS. For the vertical test of TCAS II, we take the measurement accuracy of the reported altitude into account. The accuracy of the altitude is assumed to be 25 ft, which is based on the resolution of the surveillance broadcasting [18].

When the change rate is very low, the distance can be close without a violation of the time-based tests [Eq. (24)]. To avoid that situation, an additional range test is given in which a current or a predicted relative distance to A/C 2 is compared with the minimum safety thresholds. The safety-range thresholds (SRT) are given for the horizontal threshold, distance modification (DMOD), and vertical threshold (altitude threshold), respectively, by TCAS II criteria [17]. When the intruder approaches with a constant-velocity vector, if the predicted relative distances in the horizontal and vertical directions after t_{pred} satisfy

$$r(t_c) + \dot{r}(t_c) \cdot t \triangleq r_{\text{pred}}(t_c) < \text{DMOD} \tag{25a}$$

$$r_z(t_c) + \dot{r}(t_c) \cdot t \triangleq r_{z,\text{pred}}(t_c) < \text{altitude threshold} \qquad t \in \{0, \text{Tau}\} \tag{25b}$$

then the detection system triggers an alarm. It is assumed here that the range sensor of TCAS II can measure the relative distance to an intruder approaching from any direction without measurement error.

Because it is desirable to use a more accurate model of time to CPA, a modified Tau test has been proposed, which takes the DMOD distance into account and produces less FAs [3]. The modified Tau tests for both directions are given as

$$\frac{-r}{\dot{r}}\left(1 - \left(\frac{\text{DMOD}}{r}\right)^2\right) < \text{Tau} \tag{26a}$$

$$\left| r_z - \dot{r}_z\left(\frac{r}{\dot{r}}\right) \right| < \text{altitude threshold} \tag{26b}$$

When both tests in Eqs. (26) are satisfied at the same time, a traffic alert is declared. The modified version of the Tau test produces better performance of TCAS II collision detection system, although only the basic Tau test is mentioned in the official manual published by the FAA [17].

In addition to the tests in Eqs. (25) and (26), the horizontal-miss-distance (HMD) filter is introduced in TCAS II version 7 in an effort to decrease the FAs. The HMD estimates the horizontal miss distance with respect to A/C 2 and does not apply the test when the HMD of A/C 2 is larger than DMOD. When the velocity of the aircraft is constant, the estimation of the HMD and the test can be written as

$$\text{HMD} = \sqrt{\left[r^3\left(\frac{d^2r}{dt^2}\right)\right] \Big/ \left[\left(\frac{dr}{dt}\right)^2 + r\left(\frac{d^2r}{dt^2}\right)\right]} < \text{DMOD} \tag{27}$$

By the way, the estimated HMD in Eq. (27) is smaller than true HMD for a low-relative-velocity intruder and larger for a high-relative-velocity intruder. Therefore, to avoid MAs, the test in Eq. (25) should be applied as well as the HMD filter for low-relative-velocity intruders. Note that the HMD filter is applicable to the horizontal approach only. It cannot reliably estimate the HMD for 3-D and maneuvering flight intruders. In TCAS II, the SRT in Eq. (25) and HMD filter in Eq. (27) with Eq. (25) define the shape and size of the protection volume (PV) of own aircraft, as shown in Fig. 3 [17].

2. TCAS IV

The capability of providing three-dimensional position and velocity from GPS enhances the structure of detection methods of the current TCAS. We make use of estimates of position, velocity, and attitude parameters from the PS-CP-GPS PF described in Sec. II and Appendix A.

With a constant-velocity assumption, the three-dimensional version of Eq. (25) is

$$X_{\text{pred}}(t_c) = X(t_c) + V(t_c) \cdot t \in \text{SRT}, \qquad t \in \{0, \text{Tau}\} \tag{28}$$

where $X_{\text{pred}}(t_c)$ is the predicted relative position vector of a intruder against ownship during period t and the SRT can be defined in three-dimensional space. The ability to provide three-dimensional relative information for the TCAS IV makes it possible to detect possible collision with the complete shape of the minimum safety threshold in 3-D coordinates.

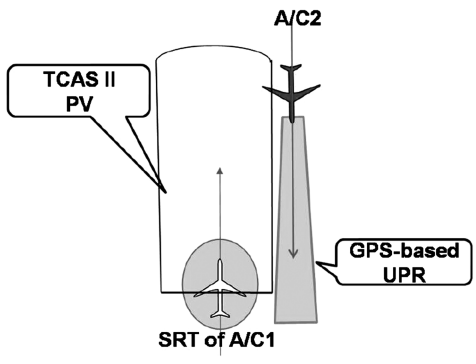

Fig. 3 Comparison of uncertainty prediction regions.

The relative states of the approaching A/C are to be placed in a convenient coordinate frame. The position and velocity vector measured in the GPS coordinate frame can be transformed into a local frame: that is, the relative navigation frame (north–east–down) or the geodetic coordinate (latitude–longitude–altitude). In this section, we use the relative navigation frame, in which the position of A/C 1, $X_1(t_c)$, is always at the origin and the future trajectory of A/C 2 at time $t > t_c$, $X_2(t)$, is relative to $X_1(t_c)$.

The true value of relative position and velocity produces a predicted position vector, and the uncertainties on the relative position and velocity vector expand the vector to a region. An error contained in the estimated position effects the origin of the position vector of an intruder and an error in estimated velocity effects the direction of the velocity vector. In fact, the combination of both errors produce a volume called the uncertain prediction region (UPR) with respect to the trajectory of the intruder. The overlapping of the intruder's UPR and own A/C's SRT is regarded as the threat for the TCAS IV. The UPR of the TCAS IV differs from the PV of TCAS II in that the UPR represents the uncertainty about a future trajectory of A/C 2 propagated according to dynamics in the relative domain, whereas the PV of TCAS II is a safety volume around A/C 1 with regard to A/C 2. The pictorial description of the UPR for the TCAS IV is compared with the PV of TCAS II in Fig. 3.

The shape of the UPR generated by both the uncertainty of position and velocity during the prediction time may be expressed by a combination of a sphere and ellipsoid in 3-D space. We apply the particle representation for constructing the UPR of TCAS IV for which the states are assumed to be approximated with normally distributed particles, for practical reasons, as

$$\mathrm{UPR}^{\,i}(t_c) = [\,X^i \quad V^i\,], \qquad i = 1, \ldots, m_s \tag{29a}$$

$$X^i \sim \mathcal{N}(\bar{X}_{12}, \Omega_{X12}), \qquad V^i \sim \mathcal{N}(\bar{V}_{12}, \Omega_{V12}) \tag{29b}$$

The mean and variances of the relative position and velocity estimation can be obtained from the PF described in Sec. II.

The UPR at t_c can be propagated using the particles in Eq. (29) as

$$R_{\mathrm{UPR}}(t_c) = \{X^i(t), i = 1, \ldots, m_s, t \in \{t_c, t_c + \mathrm{Tau}\}\} \tag{30}$$

with the simple dynamics for the constant velocity, $\dot{X}^i(t_c) = V^i(t_c)$ and $\dot{V}^i(t_c) = 0$. The detection of potential collisions are implemented by monitoring the probability of collision. The probability of collision can be estimated by the overlapped area between the UPR of the intruder and the SRT of own A/C as [19]

$$\mathrm{pr}\,(t_c) = \int_{X(t)\in \mathrm{SRT}} p(X)\mathrm{d}X \Leftrightarrow E[c(f(X(t)))] \tag{31a}$$

$$t \in [t_c, t_c + \mathrm{Tau}], \qquad c(f(X(t))) = \begin{cases} 1 & \text{if } f(X(t)) \in \mathrm{SRT} \\ 0 & \text{if } f(X(t)) \notin \mathrm{SRT} \end{cases} \tag{31b}$$

where $f(X(t))$ is the UPR during time period t, which is approximated by $R_{\mathrm{UPR}}(t_c)$ in Eq. (30). The probability of collision can be approximated by the particles for UPR using a MC approximation as

$$\widehat{\mathrm{pr}}(t_c) = \frac{1}{m_s}\sum_{i=1}^{m_s} c(R_{\mathrm{UPR}}(t_c)) \tag{32}$$

and the alarm for collision is given at time t_c if $\widehat{\mathrm{pr}}(t_c)$ is greater than the designed threshold probability ε.

3. *Monte Carlo Simulation in Constant-Velocity Flight*

The numerical experiments are implemented to analyze the condition and performance of both the TCAS II and TCAS IV with respect to the relative velocity and CPA in case the velocity vectors of own A/C and intruder A/C are a constant vector.

In the MC simulation, the collision tests involve the monitoring of the predicted tracks of neighboring intruders around own A/C that are statically located around the origin in the relative domain. A large number of trials between two A/C are performed. Each trial is characterized by relative velocity and CPA. The CPA of the trials are distributed uniformly with distances between 0 and 22,000 ft, where the FA can possibly occur. The magnitude of the relative velocity is distributed uniformly between 5 and 900 kt. One trial of the MC simulation proceeds in three steps.

1) An intruder begins to approach with a constant relative velocity.

2) As an intruder A/C approaches gradually, each detection system checks the collision using tests given in Eq. (25) for a low-relative-speed intruder, Eqs. (26) and (27) for a TCAS II detection system, and Eq. (28) for TCAS IV.

3) If an intruder cannot pass the tests, the detection system gives a warning. When an intruder reaches a predesigned CPA without the collision warning, one trial ends. We assume that the navigation information can be communicated at every computation time (i.e., 1 s) without delay in the nonterminal area. In the terminal area, the update of navigation information may be delayed, but effects of the delay in dense traffic areas is beyond the scope of this paper.

The MC simulation results, shown in Fig. 4 (left), indicate that a large number of FAs are given with regard to TCAS II. The circle, cross, and dot symbols represent no alarm for no collision, false alarm for no collision, and correct alarm for collision, respectively. The DMOD line shows the horizontal-miss-distance safety threshold. Because the DMOD is much larger than the altitude threshold, the intruder can pass by above or below the own airplane without crossing the SRT. The FA rate increases for trials in which the relative

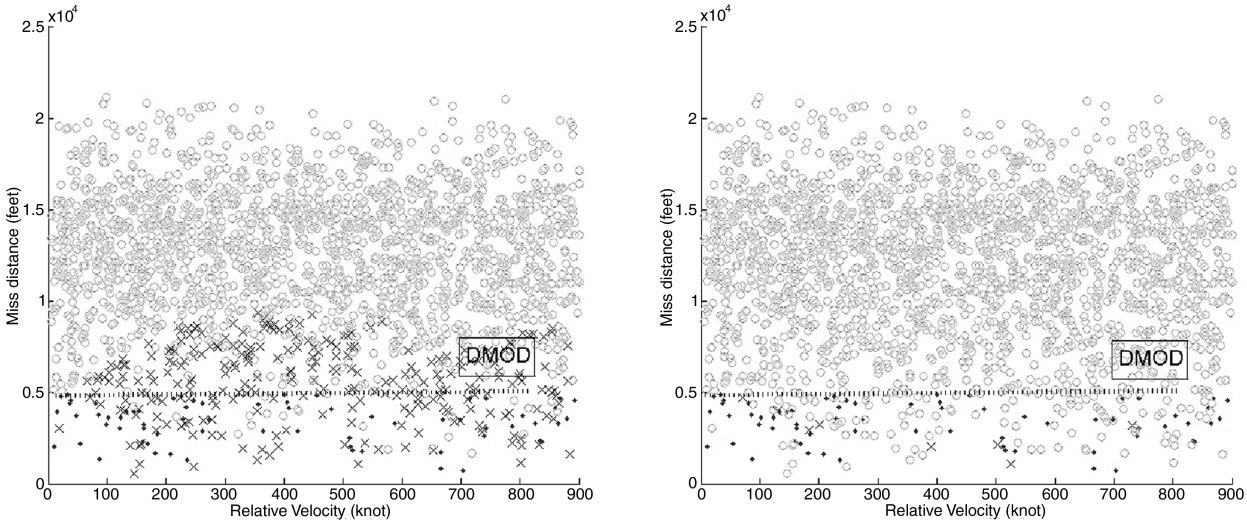

Fig. 4 False alarm zone for TCAS II (left) and III (right).

velocity is higher than 100 kt, because the estimated HMD increases for the velocity higher than 100 kt. The condition of possible FA can be observed from Fig. 4 (left). For example, when the relative closure rate is 400 kt, the TCAS II may generate a FA associated with an intruder passing by with a miss distance between 400 ft (altitude threshold) and 9500 ft.

The FA for TCAS IV is plotted in Fig. 4 (right). The simulation environment is identical to TCAS II system experiments. The position accuracy used for generating the collision UPR are 3 cm ($\approx$0.1 ft) rms for CP, and the velocity accuracy used is 3 cm/s (6 ft/m). The symbols in Fig. 4 (right) are the same as the TCAS II case. The FA takes place only around the nearby SRT of own A/C. Note that the conditions of the FA for the TCAS IV are affected only by the uncertainty of estimated relative position and estimated relative velocity, but not by the relative velocity itself. However, the FA rate of TCAS II detection is affected by the miss distance and relative velocity.

4. *Probability of False Alarm in MC Simulation*

Estimating the FA rate by the ratio of the number of FA occurrences to the number of MC trial time varies according to the distribution of the CPA of the intruder's course. In other words, if the CPA of each trial are distributed densely around the PV with the given number of total MC trials, a lower FA rate is expected, because many trials will end up with a true collision event. Therefore, to determine the probability of FAs independently of the distribution of the CPA, the results of all trials are classified according to their miss distance.

If the relative velocity range is limited between 5 and 900 kt, the FA for TCAS II can occur within the range of about 11,000 feet, as shown in Fig. 4. Therefore, we are interested in the CPAs of trials distributed within the range of 15,000 ft to the own A/C. The miss distance is divided into 30 bins, and each bin covers 500 ft. The FA probability of the bth bin is approximated separately as

$$\widehat{\mathrm{pr}}(FA(b)) = \frac{1}{m_b}\sum_{\mathrm{bi}=1}^{m_b} c(X^{\mathrm{bi}}) \tag{33}$$

where

$$c(X^{\mathrm{bi}}) = \begin{cases} 1 & \text{if } X^{\mathrm{bi}} \notin \mathrm{FA} \\ 0 & \text{if } X^{\mathrm{bi}} \in \mathrm{FA} \end{cases}$$

$b = 1, \ldots, 30$ (15,000/500), m_b is the number of trials ending up with an alarm in the bth bin, and X^{bi} is the results of the ith trial in the bth bin. The estimation of the probability is carried out separately for each bin, and the probability of FA for each bin $\widehat{\mathrm{pr}}(FA(b))$ in Eq. (33) is not dependent on the total number of trials or the distribution of the CPA. The probability of FA for each system is estimated from MC simulation using Eq. (33). The probabilities of FA estimated in Eq. (33) for the TCAS IV system and TCAS II system are shown in Fig. 5. Table 2 shows the bin numbers (relative distances) in which the FA probability is almost zero. The trends in the FA probability are not monotonic, because the shape of the SRT is not a sphere (DMOD $\gg$ altitude threshold). For GPS CP, the intruder passing by own A/C within 100 ft has a higher than 40% FA probability. However, this FA probability is not made in the most realistic setting, because the body is assumed to be a point and the actual size of the body is not considered in this simulation.

B. Maneuvering Flight

When the own airplane encounters an intruder approaching near the airport terminal area, the approaching trajectory has some curvature in either the vertical or horizontal direction or both. In that case, the future trajectory cannot be represented by only the current position and velocity. One example of the limitation of the UPR or HMD filter with a constant velocity for a parallel approach is shown in Fig. 6. The collision may not be detected in time at points 1, 2, and 3. Instead, the curvature of the approaching A/C should be predicted more precisely with 3-D attitude and angular velocity information.

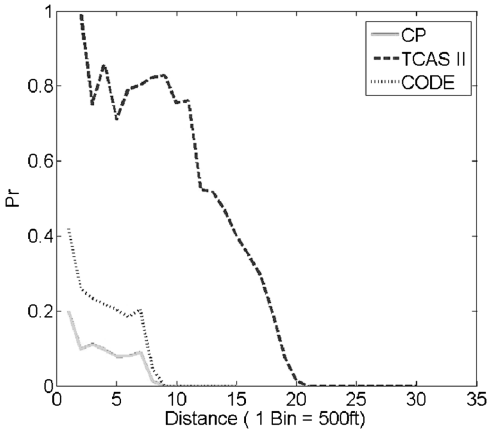

Fig. 5 Probability of false alarm for GPS-based and TCAS II detection system.

Therefore, the collision avoidance system should be analyzed for the case in which the approach trajectory of the own and intruder is not limited by the constant-velocity assumption and the own and intruder are able to change their forwarding speed and direction in either the horizontal or vertical direction or both. As mentioned at the beginning of Sec. III, the ADSB collision detection system and the TCAS II and TCAS IV are considered. When the flight motion of A/C is coupled in both the horizontal and vertical directions, the future trajectory for the ADSB system is predicted by the heading and turn rates, whereas the TCAS IV uses 3-D attitude and angular velocity, which is used to predict the 3-D maneuvering flight trajectory.

1. *TCAS II Collision Detection*

The TCAS II collision detection for maneuvering trajectories uses tests similar to the constant-flight assumption. However, the HMD filter in Eq. (27) cannot be used, because the HMD estimation is based on one-dimensional range, and the change in the range (the HMD estimate) does reflect the change of velocity vector in 3-D. Therefore, the applicable tests for the TCAS II are only Eqs. (25) and (26).

2. *TCAS IV*

System faults or human error can cause large deviation from the intended trajectory. It is especially important when the intruder approaches from a close parallel trajectory, as shown in Fig. 6. This situation should be detected as soon as possible. Attitude information (Appendix A) can be used effectively to predict this type of future trajectory.

As stated, the GPS CP measurements of the intruder are assumed to be transmitted to own ship as well as the attitude parameters represented by the Euler angles $Eu = [\phi \quad \theta \quad \psi]$ and angular velocity $\boldsymbol{\omega}$. Then the position and velocity states of intruder in navigation frames $X_{2,N}$ and $V_{2,N}$ and the coordinate transition matrix mapping a vector from a body frame to a navigation frame $A(Eu)$ are estimated using the CP measurements. The estimated state information of own A/C (i.e., A/C 1) is available at any time, whereas the information of A/C 2 is available only through broadcasting. Therefore, the accuracy of the UPR during the projected time is critically dependent on the timeliness and accuracy of information from A/C 2. We assume that the states of A/C 1 are available instantly and are treated as a true value. The transmitted data from A/C 2 determine the

Table 2 Probability of FA for TCAS IV (code, CP) and TCAS II (300/600/900 kt)

Bin number [a]	1	8	19
TCAS IV: CP, %	20	1	0
TCAS IV: code, %	41	4	0
TCAS II, %	100	82	8

[a]The relative distances is bin $\times$ 500 ft.

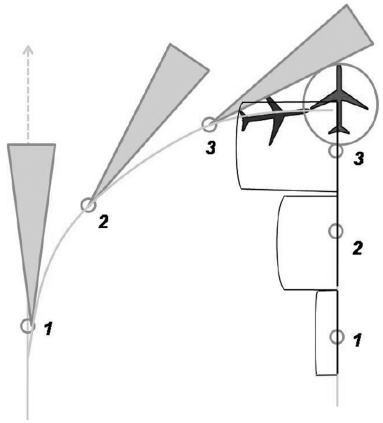

Fig. 6 Limitation of constant-velocity-based UPR.

uncertainty of the projected trajectory. The particles approximating the states of A/C 2 are

$$\text{UPR}^{\,i}(t_c) = [\,X^i \quad V^i \quad Eu^i \quad \boldsymbol{\omega}^i\,], \qquad i = 1, \ldots, m_s \tag{34}$$

$$X_N^i \sim \mathcal{N}(\bar{X}_{2,N}, \Omega_{X(2,N)}), \qquad V_B^i \sim \mathcal{N}(\bar{V}_{2,B}, \Omega_{V2,B}) \tag{35}$$

$$Eu^i \sim \mathcal{N}(\overline{Eu}, \Omega_{Eu}), \qquad \boldsymbol{\omega}^i \sim \mathcal{N}(\bar{\boldsymbol{\omega}}_2, \Omega_{\omega 2}) \tag{36}$$

where the mean and variance values can be obtained by the CP-GPS-PF navigation system as addressed in Secs. II and IV and in [11].

To properly represent the projected future trajectory, the UPR is propagated according to the available information, including the attitude parameter and angular velocity, the equations of motion for A/C 1 and A/C 2, as

$$\begin{bmatrix} \dot{X}_{1,N} \\ \dot{V}_{1,B} \\ \dot{Eu}_1 \end{bmatrix} = \begin{bmatrix} A(Eu_1)\cdot V_{1,B} \\ -\boldsymbol{\omega}_1 \times V_{1,B} \\ C(Eu_1)\cdot \boldsymbol{\omega_1} \end{bmatrix}, \qquad \begin{bmatrix} \dot{X}^i_{2,N} \\ \dot{V}^i_{2,B} \\ \dot{Eu}^i \end{bmatrix} = \begin{bmatrix} A(Eu^i)\cdot V^i_{2,B} \\ -\boldsymbol{\omega}^i \times V^i_{2,B} \\ C(Eu^i)\cdot \boldsymbol{\omega^i} \end{bmatrix} \tag{37}$$

where

$$C(Eu_1) = \begin{bmatrix} 1 & s\phi t\theta & t\theta c\phi \\ 0 & c\phi & -s\phi \\ 0 & s\phi \sec\theta & c\phi \sec\theta \end{bmatrix} \tag{38}$$

$$A(Eu_1) = \begin{bmatrix} c\theta c\psi - s\theta c\phi s\psi & -c\theta s\psi - s\theta c\phi c\psi & s\phi s\theta \\ s\theta c\psi + c\theta c\phi s\psi & -s\theta s\psi + c\theta c\phi c\psi & -s\phi c\theta \\ s\phi s\psi & s\phi s\psi & c\phi \end{bmatrix} \tag{39}$$

$X_{1,N}$ is the position of A/C 1 in the navigation frame, $V_{1,B}$ is the velocity of A/C 1 in the body frame, Eu are the Euler angles of A/C 1, and A is the transition matrix mapping a vector from the body frame to the navigation frame. The angular velocity is assumed to be constant during relative trajectory tracking. The Euler angles are used for orientation and are consistent with the navigation message.

The UPR for the relative trajectory at time t_c is approximated as

$$R_{\text{UPR}}(t_c) = \{X^i_{2,N}(t) - X_{1,N}(t), i = 1, \ldots, m, t \in [t_c, t_c + \text{Tau}]\} \tag{40}$$

Once $R^i_{\text{UPR}}(t_c)$ is computed, it is propagated up to $R^i_{\text{UPR}}(t_c + \text{Tau})$ and the UPR is updated by Eqs. (34–40) whenever new information from A/C 2 is available. The collision test is given by Eq. (32).

3. *ADSB-Based Collision Detection in Maneuvering Flight*

When a maneuvering intruder approaches, the ADSB detection system differs from the TCAS IV in that only the horizontal flight direction and the change in its direction are available. However, the TCAS IV is capable of transmitting 3-D attitude and angular velocity information. In this section, the collision detection system, based on the information assumed to follow the RTCA/DO-242A [14] for its data protocol, is discussed for a maneuvering approach trajectory.

It is assumed that yaw angle and the z-axis angular velocity can be used for heading and turn rate. This assumption is valid when the sideways velocity in the y axis of the body frame (i.e., sideslip) is small relative to the oncoming airflow. The equation of motion of A/C 1 is identical to that given in Eq. (37). When the ADSB information of A/C 2 (i.e., position, velocity, ψ, and $\omega_{2,z}$) are received, the kinematic equations of motion for A/C 2 can be obtained as

$$\begin{bmatrix} \dot{n}_2 \\ \dot{e}_2 \\ \dot{d}_2 \\ \dot{\psi} \end{bmatrix} = \begin{bmatrix} \cos(\psi)\cdot v_{2,x} + \sin(\psi)\cdot v_{2,y} \\ \sin(\psi)\cdot v_{2,x} - \cos(\psi)\cdot v_{2,y} \\ v_{2,d} \\ \omega_{2,z} + \Delta\omega_{2,z} \end{bmatrix} \tag{41}$$

where the position of A/C 2 in the navigation frame is given as $X_{2,N} = [\,n_2 \quad e_2 \quad d_2\,]^T$; the velocity in the navigation frame and in the body frame are $[\,v_{2,n} \quad v_{2,e} \quad v_{2,d}\,]^T$ and $[\,v_{2,x} \quad v_{2,y} \quad v_{2,z}\,]^T$, respectively; and $\Delta\omega_{2,z}$ is a variation in the z-axis angular velocity. In fact, the turn rate $\dot{\psi}$ in Eq. (41) is affected not only by heading rate, but also by bank angle. When the A/C has a nonzero bank angle, this bank angle cause a variation of the horizontal trajectory. The variation of $\omega_{2,z}$ from the bank angle can be written as $\delta\omega_{2,\phi} = g/|V_2|\tan(\phi)$, where g is the gravitational force, and $|V_2|$ is the norm of the velocity vector of the A/C 2. When we consider the estimation error in the transmitted angular velocity as $\delta\omega_{2,z}$, the total variation of angular velocity by the bank angle effect and angular velocity error becomes $\Delta\omega_{2,z} = \delta\omega_{2,z} + \delta\omega_{2,\phi}$. The horizontal UPR of the ADSB collision detection system is shown with a solid line in Fig. 7. For practical reasons, the UPR for the ADSB system is approximated and described by a dotted line in Fig. 7, and we restrict the maximum value of the bank angle ($\max|\phi|$) to 35 deg. Then the angle of the approximated ADSB UPR generated from the variation of $\Delta\omega_{2,z}$ is [3]

$$\delta\psi = \text{atan}\left(\frac{1 - \cos(|\Delta\omega_{2,z}|\cdot \text{Tau})}{\sin(|\Delta\omega_{2,z}|\cdot \text{Tau})}\right) \tag{42}$$

The collision test for both own and intruder can be made in the horizontal and vertical directions independently by

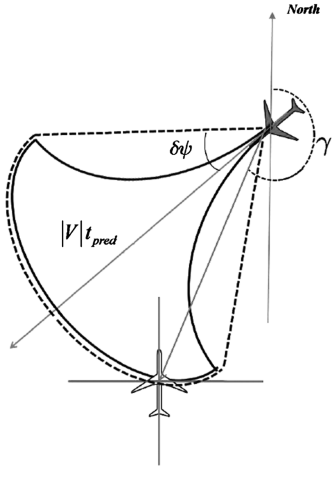

Fig. 7 UPR of ADSB collision detection system.

$$|X_{12,\text{hor}} + V_{12,\text{hor}} \cdot \text{Tau}| \le \text{DMOD}, |d_{12} + v_{12,d} \cdot \text{Tau}|$$
$$\le \text{ altitude threshold } \text{atan}\left(\frac{v_{12,e}}{v_{12,n}}\right) - \delta\psi \le \gamma$$
$$\le \text{atan}\left(\frac{v_{12,e}}{v_{12,n}}\right) + \delta\psi \tag{43}$$

where $X_{12,\text{hor}} = [\, n_{12} \quad e_{12}\,]^T$, $V_{12,\text{hor}} = [\, v_{12,n} \quad v_{12,e}\,]^T$, $\gamma = \text{atan}(e_{12}/n_{12})$, and $(\cdot)_{12} = (\cdot)_2 - (\cdot)_1$.

4. MC Simulation For Maneuvering Flight

A simulation is implemented to analyze FA and MA probabilities when the flight trajectory is not straight and level. The simulation allows the airplane to change the attitude and angular velocity so that the approach trajectory between own and intruder can reflect realistic encounters. The rms errors in Table A1 are used for the errors in the Euler angles and the angular velocity estimates. The process of simulation for each trial is similar to that of the constant-velocity case in Sec. III.A.3.

1) Both an intruder and own airplane begin to approach with a constant relative velocity. The magnitude of the velocity of each A/C is distributed uniformly between 50 and 400 kt.

2) The own airplane predicts the UPR using Eqs. (34–40) for TCAS IV and using Eqs. (41) and (42) for the ADSB-based system.

3) Either own or intruder or both start to make a turn with an angular velocity $\boldsymbol{\omega}_1$ for the own airplane and $\boldsymbol{\omega}_2$ for the intruder at t_{turn} seconds before both reaching the CPA, where t_{turn} is uniformly distributed between 5 and 30 s; $\boldsymbol{\omega}_i$ $(i = 1, \text{or } 2)$ for three directions in the body frame are distributed uniformly in $[-0.1, 0.1]$ deg/s.

4) As the intruder A/C approaches or becomes more distant by gradually turning, each detection system checks the collision using tests given in Eqs. (25) and (26) for TCAS II, the test in Eq. (43) for ADSB-based, and the test in Eq. (32) for TCAS IV at each current time t_c.

5) If an intruder cannot pass one of any the tests, the corresponding detection system gives a warning. When the distance rate to the intruder turns positive without a collision warning, the trial ends.

6) After a number of MC trials are finished, the probabilities of FA and MA for each system are estimated by Eq. (33).

When both own and intruder approaches are maneuvering, the FA and MA rates are determined by a combination of several factors such as miss distance, relative velocity, turn rate, turning point, data link update frequency, etc. Therefore, the FA and MA zones cannot be characterized as in the constant-velocity case shown in Fig. 4. Table 3 shows the FA and MA rates for a MC simulation with over 30,000 trials. In the maneuvering flight, the FA probability represents a ratio of the unnecessary alarm over the total number of alarms. A 4-sigma (99.99%) standard deviation is used for the error of the CP-based position and velocity estimates in the simulation for TCAS IV to ensure reliability. As a result, no MA occurred during simulation, whereas the FA rate is increased.

Even though the SRT test in Eq. (25) of TCAS II generates high FAs, the test is essential to avoid the MA with regard to low-relative-velocity A/C. The reason for the increase in the FA probability for the TCAS II in Table 3 is that the HMD filter is not used for the maneuvering flight. The ADSB-based system has a MA with a 0.004% probability. This event occurs when the navigation message at discrete time t_{k-1} predicts a distance that is very close to the PV when in straight and level flight, but at time t_k, the intruder makes a steep turn and touches or passes through the boundary of the PV of the own airplane. However, the collision avoidance system cannot detect this contact until time t_{k+1}, because the information is assumed to be transmitted at 0.5 Hz. This situation cannot be avoid by more accurate navigation data, but by a faster message update rate. To avoid MA occurrence, airplanes in the close vicinity should transmit the ADS-B messages to each other with a higher communication rate.

Table 3 FA/MA probability comparison (30,000 trials)

	FA[a]	MA[a]	FA[b]	MA[b]
TCAS II, %	31.638	0	74.921	0
TCAS IV[c], %	1.332	0	22.349	0
ADSB, %	——	——	73.585	0.004

[a]Constant velocity. [b]Maneuvering. [c]GPS CP.

IV. Conclusions

A new robust and practical approach for estimating the navigation states using CP (carrier phase) is addressed, and a CP-GPS-based airborne collision detection system is presented for the next-generation air traffic alert and collision avoidance system. The CP-GPS-based collision detection system (TCAS IV) is compared with the current TCAS (TCAS II) system and the ADSB-based collision detection system. The FA (false alarm) and MA (miss alarm) probabilities of each collision detection system are determined through MC (Monte Carlo) simulations.

The PF approach is used for the GPS CP navigation estimation problem to handle the integer ambiguity problem. The samples are drawn from the 3-D position space coordinates, and so the GPS CP navigation system is insensitive to changes of the available GPS satellites and cycle slips. Therefore, the position-sample-based PF is more robust in realistic operations than the traditional integer-ambiguity-resolution-based CP algorithms. Furthermore, the PS-CP-GPS can combine the geometry of multiple antennas directly into the attitude determination for additional redundancy and fast convergence performance.

To take full advantage of GPS CP measurements in the collision detection system, we assume that the information transmitted by the collision detection system includes the GPS CP measurements, rather than transmitting only estimated navigation states. In doing so, two major benefits are addressed: accuracy and redundancy.

1) Because of the inaccuracy of the current TCAS II, the TCAS II detection system is not used when precise navigation and detection are required. For example, TCAS II does not issue advisories for the intruders for which the altitude is lower than 360 ft and is therefore not usually used for the landing or takeoff phases [2]. The relative position and velocity between one antenna on own airplane and another antenna on the intruder were estimated as accurately with a mean and rms errors of relative position less than 1 cm (0.15 ft) and 2.1 cm (0.32 ft), respectively. Therefore, the CP-GPS-based (with PS-CP-GPS PF) collision detection system can provide an accurate collision detection method.

2) Because the accuracy of the GPS CP relative position estimates is not susceptible to the accuracy of the absolute position estimates by the code, the GPS CP collision detection system provides independent redundant information in addition to the GPS code-based detection.

The prediction of the intruders trajectory can be made based on the estimated navigation states. As noted, the attitude and angular velocity of the intruder are estimated by the GPS navigation system of each airplane and transmitted to other airplanes as well as CP measurements. Then the relative position and velocity of own to the intruder are estimated based on the transmitted CP measurements from the intruder. The error in the navigation states introduces a variation in the predicted trajectory. If an intruder approaches with a constant velocity on a collision course, both the TCAS II and TCAS IV (CP) can detect the intruder with 100% probability. However, TCAS II and TCAS IV generate 31.6 and 1.3% probability of a FA in the same MC simulation, respectively. When the intruder and own airplane approach with a curved maneuvering trajectory, the TCAS IV predicts the trajectory using the attitude information of the own and intruder to predict the future trajectory more precisely. The TCAS IV shows less than a 23% (0%) probability of FA (MA), whereas the TCAS II and the ADSB-based system show about 75% (0%) and 74% (0.004%) probabilities of a FA (MA), respectively.

Because TCAS II or the ADSB-based system do not provide accurate three-dimensional attitude information, these collision detection systems should apply the worst-case assumptions to overcome their limitations. Although this assumption is required for a zero-miss alarm rate, a large number of unnecessary alarms are inevitable.

Therefore, transmitting the attitude information as well as the CP measurements for precise position and velocity estimates between nearby airplanes can enhance the precise tracking of the approach trajectory for reliable collision detection and decrease FA rates significantly.

Appendix A: Attitude Determination

I. Baseline Vector Estimation in Position Coordinate Space

Consider the relative position from the primary antenna (i.e., antenna 1) to the secondary antennas (i.e., antenna i, where $i = 1, \ldots, n_B$) on the body of own airplane in the inertial frame δX_i. Each secondary antenna provides one baseline vector. When the body rotates with the angular velocity and no other external source of the angular velocity is assumed, the angular velocity should be included in the state as well. The baseline vectors and the angular velocity are considered in augmented states as

$$\mathbf{X}_a \triangleq [\,\delta X_1 \quad \delta X_2 \quad \cdots \quad \delta X_{n_B} \quad \boldsymbol{\omega}\,] \tag{A1}$$

The dimension of $\mathbf{X}_a$ in Eq. (A1) is $3 \cdot (n_B + 1)$ by 1.

If it is assumed that the body is rigid and the antenna's geometry in the body frame is known, $\mathbf{X}_a$ can be simplified. For example, suppose that the GPS antennas are arranged as an orthogonal tripod. Then the geometry relationship among the baseline vectors can be written as

$$|\delta X_1| = |\delta X_2| = |\delta X_3| = b \tag{A2a}$$

$$\delta X_1 \cdot \delta X_2 = \delta X_1 \cdot \delta X_3 = 0 \tag{A2b}$$

$$\delta X_3 = \delta X_1 \times \delta X_2 \tag{A2c}$$

If three components of the first baseline vector $\delta X_1 = [\delta x_1, \delta y_1, \delta z_1]T$ are given, only two components of δX_2 are required to express δX_2 and the other baseline vectors δX_i $(i = 3, \ldots, n_B)$. For example, we additionally pick δx_2 and δy_2 for δX_2, then δX_2 and δX_3 can be expressed as

$$\delta X_2 = b\frac{\underline{X}_2}{|\underline{X}_2|} \tag{A3}$$

where

$$\underline{X}_2 = \{\,\delta x_2 \quad \delta y_2 \quad \delta z_2\,\}^T = \left\{\,\delta x_2 \quad \delta y_2 \quad \frac{-\delta x_1 \delta x_2 - \delta y_1 \delta y_2}{\delta z_1}\right\}^T$$

$$\delta X_3 = b\frac{\underline{X}_3}{|\underline{X}_3|} \tag{A4}$$

where

$$\underline{X}_3 = \delta X_1 \times \delta X_2$$

In this way, the augmented state $\mathbf{X}_a = [\,\delta X_1, \quad \delta X_2, \quad \delta X_3, \quad \boldsymbol{\omega}\,]^T$ can be expressed by only five parameters ($\delta x_1, \delta y_1, \delta z_1, \delta x_2$, and δy_2) and the angular velocity of the body $\boldsymbol{\omega}$. This simplification holds for arbitrary but known antenna geometry. The simplified state is written as

$$\tilde{\mathbf{X}}_a = [\,\delta x_1 \quad \delta y_1 \quad \delta z_1 \quad \delta x_2 \quad \delta y_2 \quad \boldsymbol{\omega}^T\,]^T \tag{A5}$$

The augmented state $\mathbf{X}_a$ is now a function of the simplified augmented state $\tilde{\mathbf{X}}_a$. Consequently, the estimate of n_B baseline vectors reduces to estimating eight parameters in the simplified augmented state. Both $\mathbf{X}_a$ and $\tilde{\mathbf{X}}_a$ can be used to represent the baseline vectors. Note that the ambiguity-based algorithms make use of the baseline distance, whereas the position sample PF makes use of not only the baseline distance, but also the geometries between antennas.

In the attitude determination using the PF, the pdf of the state is approximated using the kinematic equation (A6) and the n_B-augmented CP measurements equation (A7). The baseline vectors on the rigid body rotate with the body frame. The rate of change of the state is given as

$$\dot{\mathbf{X}}_a = \begin{bmatrix}\delta V \\ \boldsymbol{\alpha}\end{bmatrix} = \begin{bmatrix}\delta V_1 \\ \delta V_2 \\ \vdots \\ \delta V_{nB} \\ \boldsymbol{\alpha}\end{bmatrix} = \begin{bmatrix}\boldsymbol{\omega} \times \delta X_1 \\ \boldsymbol{\omega} \times \delta X_2 \\ \vdots \\ \boldsymbol{\omega} \times \delta X_{nB} \\ \dot{\boldsymbol{\omega}}\end{bmatrix} \tag{A6}$$

Now each particle is sampled to represent $\tilde{\mathbf{X}}_a$, which represents the full state $\mathbf{X}_a$. Because $\tilde{\mathbf{X}}_a$ has only eight independent parameters for the n_B baseline vectors, each sample has eight dimensions. The initial samples for the state can be drawn from the initial estimates by the code measurements. The details of initial baseline estimation by the code and Doppler measurements are discussed in Sec. II. The number of independent samples m_s at time $k = 0$ is obtained by picking m_s independent and identically distributed samples distributed uniformly. Note that the A/C in this paper starts in a constant vector flight mode and the initial $\boldsymbol{\omega}$ used is $[\,0, \quad 0, \quad 0\,]^T$. Then each particle for the simplified augmented states $\mathbf{X}_a^i$ can be obtained from corresponding particle $\tilde{\mathbf{X}}_a^i$ using the relationships in Eqs. (A3) and (A4).

The augmented CP measurement equations for n_B baselines is similar to Eq. (14) as

$$z_k = \begin{bmatrix}\nabla\Delta\Phi_1 \\ \nabla\Delta\Phi_2 \\ \vdots \\ \nabla\Delta\Phi_{n_B}\end{bmatrix} = \begin{bmatrix}\nabla\Delta\varrho_1 \\ \nabla\Delta\varrho_2 \\ \vdots \\ \nabla\Delta\varrho_{n_B}\end{bmatrix} - \lambda\begin{bmatrix}\nabla\Delta N_1 \\ \nabla\Delta N_2 \\ \vdots \\ \nabla\Delta N_{n_B}\end{bmatrix} + \begin{bmatrix}\nabla\Delta\eta_1 \\ \nabla\Delta\eta_2 \\ \vdots \\ \nabla\Delta\eta_{n_B}\end{bmatrix} \tag{A7}$$

$$\nabla\Delta\Phi = \nabla\Delta\varrho - \lambda \cdot \nabla\Delta N + \nabla\Delta\eta \tag{A8}$$

where $\nabla\Delta\Phi_i$, $\nabla\Delta\varrho_i$, $\nabla\Delta N_i$, and $\nabla\Delta\eta$ represent the DD CP measurements, the DD range, DD ambiguity, and DD CP noise vector for the ith baseline, respectively. Note that we use the same symbols of $\nabla\Delta\Phi$, $\nabla\Delta\varrho$, $\nabla\Delta N$, and $\nabla\Delta\eta$ for both the single-baseline and multibaseline cases. The dimension of the vectors $\nabla\Delta\Phi$, $\nabla\Delta\varrho$, $\nabla\Delta N$, and $\nabla\Delta\eta$ in Eq. (A7) is $n_B \cdot (n_s - 1)$, where n_s is the number of GPS satellites.

The integer ambiguity estimates for the samples for all baseline can be obtained, similar to Eq. (18), as

$$\nabla\Delta\underline{N}^i = \left\lfloor \frac{1}{\lambda}(\nabla\Delta\varrho^i - \Phi) \right\rfloor_{\text{round off}}, \qquad i = 1, \ldots, m_s \tag{A9}$$

Similarly, the linearized CP measurement equation (15) can be written for multibaseline vectors as

$$\nabla\Delta\varrho_o + A_m\mathbf{X}_a = \nabla\Delta\Phi + \lambda \cdot \nabla\Delta N + \nabla\Delta\eta \tag{A10}$$

where

$$A_m = \begin{bmatrix} A_{d1} & 0 & 0 & 0 & 0 \\ 0 & A_{d2} & 0 & 0 & 0 \\ & & \ddots & & \\ 0 & 0 & & 0 & 0 \\ 0 & 0 & 0 & A_{dn_B} & 0 \end{bmatrix} \tag{A11}$$

and A_{di} is the direction matrix for DD measurements of the ith baseline. The dimension of A_{di} and zeros in Eq. (A11) is $(n_s - 1)$ by 3. Because the baseline vector length is much smaller than the GPS satellite's altitude, the differences between A_{di} are ignorable, and the same A_d defined in Eq. (11) can be used for all A_{di}.

The ambiguity from the linearized measurements equation can be computed by multiplying the null space matrix of the augmented direction cosine matrix A_m to Eq. (A10):

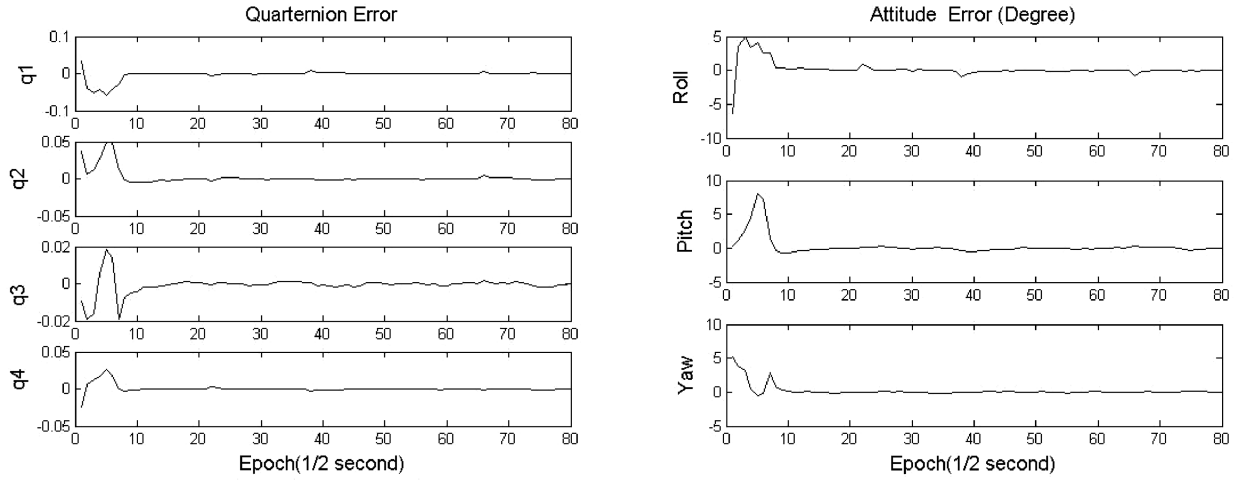

Fig. A1 Euler error (in degrees).

$$E_m^T \cdot \nabla\Delta N_L = E_m^T \cdot \nabla\Delta(\varrho_0 - \Phi - \eta)/\lambda \tag{A12}$$

where

$$E_m^T = \text{diag}(E_1^T, E_2^T, \ldots, E_{n_B}^T) = \text{diag}(E^T, E^T, \ldots, E^T)$$

E_i is a left annihilator, which eliminated the direction matrix such that $E_i^T \cdot A_{di} = 0$. Because all A_{di} are the same, E_i^T can be replaced by same E^T as in Eq. (16).

The likelihood density of each sample at time k is given as

$$p(z_k|\mathbf{X}_k^i) = C_1 \exp\{-\tfrac{1}{2}(r^i)^T (E_m^T \Omega_{\nabla\Delta N_L} E_m)^{-1}(r^i)\} \tag{A13}$$

where

$$r^i = \lambda E_m^T(\nabla\Delta\underline{N}_i - \nabla\Delta N_L) \tag{A14}$$

Finally, following the same processes as in Eqs. (20) and (23) leads to the estimates of the state.

Once the baseline vector estimate is given in the inertial coordinate frame, the attitude determination is considered as in Wahba's problem [20]. Wahba's problem is to find the orthogonal matrix $A(\mathbf{q})$ as a function of a quaternion that minimizes the loss function:

$$J(A) = \frac{1}{2}\sum_{i=1}^{n_B} W_i |X_{\text{bi}} - A \cdot \delta X_i|^2 \tag{A15}$$

where the baseline vectors in the body frame are written as X_{bi} $(i = 1, \ldots, n_B)$, n_B is the number of baseline vectors, and W_i represents the weight. The q method in the next section is used to estimate the quaternion among many solution suggested for Wahba's problem in this paper, because the q method is the first one used practically and widely [21] and does not suffer from a singularity problem. It is well known that the Euler angle method is not stable when the attitude varies more than 90 deg. Therefore, the quaternion parameters are considered during estimating and are transformed into Euler angles for reliability.

II. *q* Method

The q method is an optimal way to estimate attitude matrix $A(\mathbf{q})$ as a function of the quaternion with $n_B \geq 2$ vector observations. The loss function in Eq. (15) can be rewritten as

$$J(A) = \frac{1}{2}\sum_{i=1}^{n_B} W_i (X_{\text{bi}} - A \cdot \delta X_i)^T (X_{\text{bi}} - A \cdot \delta X_i) \tag{A16a}$$

From the property of the transition matrix, $A^T A = I_{3\times 3}$. The minimization problem of $J(A)$ becomes that of maximizing as

$$\max g(A) \triangleq \max_A \sum_{i=1}^{n_B} (\underline{X}_{\text{bi}}^T A \underline{\delta X}_i) \tag{A17}$$

where $\underline{X}_{\text{bi}} = \sqrt{W_i} X_{\text{bi}}$ and $\underline{\delta X}_i = \sqrt{W_i}\delta X_i$.

Parameterizing $A(\mathbf{q})$ with the unit quaternion $\mathbf{q}$ as [22]

$$A(\mathbf{q}) = \begin{bmatrix} 2(q_1^2 + q_4^2) - 1 & 2(q_1 q_2 - q_3 q_4) & 2(q_1 q_3 + q_2 q_4) \\ 2(q_1 q_2 + q_3 q_4) & 2(q_2^2 + q_4^2) - 1 & 2(q_2 q_3 - q_1 q_4) \\ 2(q_1 q_3 - q_2 q_4) & 2(q_2 q_3 + q_1 q_4) & 2(q_3^2 + q_4^2) - 1 \end{bmatrix} \tag{A18}$$

one solution of Wahba's problem is given as a normalized eigenvector associated with the largest positive eigenvalue of K, such that

$$g(A) = \mathbf{q}^T K \mathbf{q} \tag{A19a}$$

where

$$K = \begin{bmatrix} S - \sigma I & Z \\ Z^T & \sigma \end{bmatrix}_{4\times 4}, \qquad Z = \begin{bmatrix} B_{23} - B_{32} \\ B_{31} - B_{13} \\ B_{12} - B_{21} \end{bmatrix} \tag{A19b}$$

$$S = B + B^T, \qquad \sigma = Tr(B) \tag{A19c}$$

$$B \triangleq [\,\underline{X}_{b1} \quad \cdots \quad \underline{X}_{bn_B}\,] \cdot [\,\underline{\delta X}_1 \quad \cdots \quad \underline{\delta X}_{n_B}\,]^T \tag{A19d}$$

where B_{ij} is the $\{i, j\}$th argument of the matrix B.

III. Simulation Results of Attitude Determination

Simulation results are presented for the attitude determination using PS-CP-GPS PF with multiple antennas. Four antennas are used to estimate the attitude of an airplane on level flight. The geometries of the antennas are the same orthogonal tripod as given in Eq. (A2),

Table A1 Attitude error estimate

Parameter	Mean				RMS			
Euler, deg[a]	0.0967	0.0069	−0.0476	——	0.6810	0.4921	0.6163	——
Quaternion[b]	−0.0000	0.0002	−0.0001	0.0002	0.0008	0.0006	0.0007	0.0005
Angular velocity, deg/s	0.0009	0.0005	−0.0002	——	0.0022	0.0028	0.0027	——

[a]Roll, pitch, and yaw. [b]$q1$, $q2$, $q3$, and $q4$, deg/s.

and the baseline length between antennas is 2 m (6.56 ft) for all antennas. Other simulation inputs such as data frequency, errors in the simulation measurements, etc., used for attitude determination are the same as the data used in Sec. II.E. Figure A1 shows the error of the estimated quaternion and the error of the Euler angles transformed from the quaternion estimates. The mean error and rms error for the Euler angles and quaternion estimates are shown in Table A1.

Acknowledgment

This work was partially supported by NASA Ames Research Center grant NNA06CN22A.

References

[1] Parkinson, B. W., and Spilker, J. J., Jr. (eds.), *Global Positioning System: Theory and Practice*, Vols. 1, 2, Progress in Astronautics and Aeronautics, Vol. 146, AIAA, Washington, D.C., 1996.

[2] Reingold, L., "TCAS: Not-Quite-Perfect," *Air Transport World*, Vol. 29, No. 1, Jan. 1992, pp. 78–80.

[3] Gazit, R. Y., and Powell, J. D., "Aircraft Collision Avoidance Based on GPS Position Broadcasts," Ph.D. Thesis, Stanford Univ., Stanford, CA, Aug. 1996.

[4] Barrows, A. K., Enge, P., Parkinson, B. W., and Powell, J. D., "Flight Tests of a 3-D Perspective-View Glass-Cockpit Display for General Aviation Using GPS," *ION GPS 1995*, Inst. of Navigation, Manassas, VA, Sept. 1995, pp. 1615–1622.

[5] "Principles and Practice of GPS Surveying," Sept. 1999, http://www.gmat.unsw.edu.au/snap/gps/gps_survey/principles_gps.htm [retrieved 4 May 2009].

[6] Gu, X., and Lipp, A., "DGPS Positioning Using Carrier Phase for Precision Navigation," *Position Location and Navigation Symposium*, Inst. of Electrical and Electronics Engineers, Piscataway, NJ, Apr. 1994, pp. 410–417.

[7] Hatch, R., "The Synergism of GPS Code and Carrier Measurements," *Third International Geodetic Symposium on Satellite Doppler Positioning*, Vol. 2, New Mexico State Univ., Las Cruces, NM, 1983, pp. 1213–1231.

[8] Hofmann-Wellenhof, B., Lichtenegger, H., and Collins, J., *Global Positioning System: Theory and Practice*, 4th ed., Springer–Verlag, New York, 1997.

[9] Kim, D., and Langley, R. B., "GPS Ambiguity Resolution and Validation: Methodologies, Trends and Issues," *7th GNSS Workshop—International Symposium on GPS/GNSS*, Seoul National Univ., Seoul, (ROK), Nov. 2000, pp. 213–221.

[10] Rubin, D. B., *Using the SIR Algorithm to Simulate Posterior Distributions in Bayesian Statistics 3*, Oxford Univ. Press, Cambridge, MA, 1988.

[11] Hwnag, S. S., and Speyer, J. L., "Relative GPS Carrier-Phase Positioning Using Particle Filters with Position Samples," *Proceedings of the 2009 American Control Conference*, Inst. of Electrical and Electronics Engineers, Piscataway, NJ, June 2009.

[12] Wolfe, J. D., Williamson, W., and Speyer, J. L., "Hypothesis Testing for Resolving Integer Ambiguity in GPS," *ION GPS 2001*, Inst. of Navigation, Manassas, VA, Sept. 2001, pp. 1522–31.

[13] Klobuchar, J. A., "Ionospheric Effects on GPS," *Global Positioning System: Theory and Applications*, edited by B. W. Parkinson and J. J. Spilker Jr., Vol. 1, AIAA, Washington, D.C., 1996, Chap. 12.

[14] "Minimum Aviation Performance Standards for Automatic Dependent Surveillance Broadcasts (ADS-B)," Radio Technical Commission for Aeronautics, Std. RTCA/DO-242A, Washington, D.C., 2002.

[15] Barhydt, R., and Warren, A. W., "Development of Intent Information Changes to Revised Minimum Aviation System Performance Standards for Automatic Dependent Surveillance Broadcast (RTCA/DO-242A)," NASA TM-2002211669, 2002.

[16] Paielli, R. A., Erzberger, H., Chiu, D., and Heere, K. R., "Tactical Conflict Alerting Aid for Air Traffic Controllers," *Journal of Guidance, Control, and Dynamics*, Vol. 32, No. 1, Jan.–Feb. 2009, pp. 184–193. doi:10.2514/1.36449

[17] "Introduction to TCAS II Version 7," U.S. Department of Transportation and Federal Aviation Administration, Nov. 2000, http://www.arinc.com/downloads/tcas/tcas.pdf [retrieved 2009].

[18] Love, W. D., "Preview of TCAS II Version 7," *Air Traffic Control Quarterly*, Vol. 6, No. 4, 1998, pp. 231–247.

[19] Blackmore, L., "A Probabilistic Particle Control Approach to Optimal, Robust Predictive Control," *AIAA Guidance, Navigation, and Control Conference*, AIAA, Reston, VA, 2006.

[20] Wahba, G., "A Least Squares Estimate of Spacecraft Attitude," *SIAM Review*, Vol. 7, July 1965, p. 409. doi:10.1137/1007077

[21] Wertz, J. R., *Spacecraft Attitude Determination and Control*, Vol. 73, D. Reidel, Dordrecht, The Netherlands, 1978.

[22] Keat, J., *Analysis of Least-Squares Attitude Determination Routine DOAOP*, Computer Sciences Corp., Rept. CSC/TM-77/6034, Silver Spring, MD, Feb. 1977.